POLITECNICO DI TORINO
Repository ISTITUZIONALE

Incoming windblown sand drift to civil infrastructures: A probabilistic evaluation

(Article begins on next page)

25 April 2024

Incoming windblown sand drift to civil infrastructures: a probabilistic evaluation

Lorenzo Raffaele[a,d,*], Luca Bruno[a,d], Davide Fransos[b,d], Franco Pellerey[c]

[a]*Politecnico di Torino, Department of Architecture and Design, Viale Mattioli 39, I-10125, Torino, Italy*
[b]*Optiflow Company, Chemin de la Madrague-Ville 160, F-13015, Marseille, France*
[c]*Politecnico di Torino, Department of Mathematical Sciences, Corso Duca degli Abruzzi 24, I-10129, Torino, Italy*
[d]*Windblown Sand Modeling and Mitigation joint research group, Italy-France*

Abstract

The accurate prediction of windblown sand drift events approaching human infrastructures and activities is fundamental in arid lands. In both scientific literature and technical practice sand drift estimation is carried out in mean terms. Typically, sand drift net direction and intensity are assessed by means of the resultant drift potential. However, windblown sand suffers a number of epistemic and aleatory uncertainties, related to both the wind and the sand fields. The windblown sand drift estimation in probabilistic terms is useful in the infrastructure design perspective and allows to obtain characteristic values of windblown sand transport. In this study windblown sand is considered as an environmental action in analogy to wind action. Several uncertainties involved in the phenomenon are considered: threshold shear velocity and 10-minute average wind velocity are assumed as random variables. Monte Carlo approach is adopted within a bootstrapping technique in order to assess sand drift in probabilistic terms. The proposed approach is applied to five sites in the Arabian Peninsula. Directional statistics of the sand drift are given for each site.

Keywords: windblown sand, drift potential, uncertainty quantification, probabilistic approach, Monte Carlo

Nomenclature

DP	Drift Potential
HW	Hybrid Weibull
MC	Monte Carlo
RDD	Resultant Drift Direction
RDP	Resultant Drift Potential
SD-WA	Sand Deterministic - Wind Averaged
SWP	Sand Wind Probabilistic
D	drift potential
F	probability distribution function
F_0	wind calm rate
N	number of occurrences
Q	sand transport rate
R	resultant drift potential
T	reference time
T_r	recording time
U	wind velocity
U_{10}	10-min averaged wind speed

*Corresponding author. Tel: (+39) 011.090.4870. Fax: (+39) 011.090.4999.
Email address: lorenzo.raffaele@polito.it (Lorenzo Raffaele)
URL: http://www.polito.it/wsmm (Lorenzo Raffaele)

$c.o.v.$	coefficient of variation
d	sand grain diameter
d_r	sand grain reference diameter
f	probability density function
g	gravitational acceleration
k	Weibull shape parameter
p	percentile
sk	skewness
u_*	shear velocity
u_{*t}	threshold shear velocity
z_0	roughness length
Δt	sampling interval
$\Delta \theta$	sector width
θ	wind direction
λ	Weibull scale parameter
μ	mean value
ρ_a	air density
ρ_b	packed bulk sand density
σ	standard deviation
#	cardinality
0	calm wind

1. Introduction

Windblown sand is of interest for several engineering fields in arid environments (e.g. Middleton and Sternberg, 2013; Stipho, 1992), from environmental to civil engineering. In particular, windblown sand interacts with a number of civil structures and infrastructures, such as roads (e.g. Redding and Lord, 1981; Dong et al., 2004), railways (e.g. Zhang et al., 2007, 2010; Cheng and Xue, 2014), industrial facilities and pipelines (e.g. Alghamdi and Al-Kahtani, 2005), farms (e.g. Wang et al., 2010), town an buildings (e.g. Rizvi, 1989; Bofah and Al-Hinai, 1986). Windblown sand transport results from soil erosion and involves sedimentation around built obstacles. In particular, windblown sand effects on civil structures comprehend, but are not limited to: wind erosion and foundation scouring, moving sand dunes encroaching infrastructures, sand accumulation around structures and infrastructures. Due to the nature of these effects, they can lead to several incremental costs in infrastructure management, e.g. loss of capacity and increased maintenance costs (Zakeri, 2012), but also to disastrous events, such as train derailment (Cheng et al., 2015). The design of such infrastructures requires the accurate estimation of the amount of incoming windblown sand that attacks the structure. It significantly vary in space and time. Indeed, on the one hand, line-like infrastructures cross different regions with a wide variety of geomorphological characteristics. On the other hand, infrastructure design must ensure the service life prescribed by standards. Hence, a probabilistic approach to design is necessary to take into account the inborn variability of the phenomenon.

The amount of incoming windblown sand is defined as the mass per unit time and per unit length, and usually called *incoming sand drift*. Phenomenologically, windblown sand is a multi-physics phenomenon which includes wind and sand subfields. Hence, sand drift depends on both the wind velocity and the sand characteristics. The modelling framework to sand drift evaluation has been first introduced by Fryberger and Dean (1979). Their seminal work still grounds the current scientific and technical literature in several application fields, such as fundamental research (e.g. Al-Awadhi and Al-Awadhi, 2009; Barchyn and Hugenholtz, 2011), geomorphology (e.g. del Valle et al., 2008; Bogle et al., 2015; Kilibarda and Kilibarda, 2016; Yang et al., 2016), paleo sedimentology (e.g. Yang et al., 2014), climatology (e.g. Bogle et al., 2015), coastal management (e.g. Riksen et al., 2016), civil engineering (e.g. Dong et al., 2004; Zhang et al., 2010; Cheng et al., 2015). In the Fryberger and Dean (1979) framework, the so-called Drift Potential (DP) is defined for each wind direction, while the Resultant Drift Potential (RDP) and the Resultant Drift Direction (RDD) stand for the magnitude and direction of the vector sum of DP over the directions, respectively. These quantities are called "potential" because they provide a measure of sand-moving capacity of the wind blowing

over an ideal sand bed, neglecting the local covering of the ground surface (Pye and Tsoar, 2009). Fryberger and Dean (1979) obtain DP per reference time (usually 1 year) by cumulating the sand transport rate Q over the wind speed recording time, and rescaling it on the reference time. In turn, Q results from the vertical integration of the horizontal windblown sand flux. Several semi-empirical models to predict Q have been proposed so far, reviewed e.g. in Dong et al. (2003); Kok et al. (2012); Sherman and Li (2012). Among them, modified Bagnold type models are the most widely adopted in literature (see for instance the field studies by Fryberger and Dean, 1979; Al-Awadhi and Al-Awadhi, 2009; Barchyn and Hugenholtz, 2011; Sherman and Li, 2012; Sherman et al., 2013; Yang et al., 2014; Liu et al., 2015). In particular, the model proposed by Lettau and Lettau (1978) is the most adopted one. They all relate Q to the wind shear velocity u_* and the threshold shear velocity u_{*t}, that is the shear velocity above which sand transport occurs. Usually, such a threshold is assessed as a function of the sand grain diameter d by means of semi-empirical expressions (e.g. Bagnold, 1941; Iversen and White, 1982; Shao and Lu, 2000; McKenna, 2003). According to the Authors, it is worth pointing out that the current approach within the Fryberger and Dean (1979) framework is:

- deterministic with respect to the sand subfield. Indeed, the expressions of the threshold shear velocity u_{*t} used so far are purely deterministic;

- time-averaged with respect to the wind subfield. The wind speed inborn variability is accounted for, but only the mean value of DP is retained because the rescaling on the reference time is tantamount to averaging.

Let us call such approach as Sand Deterministic - Wind Averaged (SD-WA).

Despite SD-WA approach is generalized in practice, windblown sand phenomenon is affected by several sources of uncertainty. They can be generally classified in *aleatory* and *epistemic* uncertainties (Zio and Pedroni, 2013). Let us introduce a complementary categorization referring to the wind and sand subfields introduced above. *Epistemic* uncertainties are associated with the lack of knowledge about the properties and conditions of the phenomena to be modeled. They can be further ascribed to model, parameter and measurement uncertainties. Wind-field epistemic uncertainties are generally well quantified, because of its long-standing modelling, while sand-field ones have been only recently highlighted with respect to threshold shear velocity (e.g. Barchyn and Hugenholtz, 2011; Raffaele et al., 2016) and sand transport rate (e.g. Barchyn et al., 2014). *Aleatory* uncertainties refer to inherent randomness of natural phenomena. Let us introduce a further categorization referring to the wind and sand subfields introduced above. Wind-related aleatory uncertainties affect the velocity and other environment variables. Sand-related aleatory uncertainties take place at both the microscopic scale, i.e. grain irregular shape, grain size distribution, grain relative position on the sand bed (e.g. Nickling, 1988; Duan et al., 2013; Edwards and Namikas, 2015), and the macroscopic scale, i.e. soil vegetation covering, soil sediment availability, soil moisture and soil crusting (see e.g. McKenna Neuman and Nickling, 1989; Lancaster and Baas, 1998; Shao, 2008; Hoonhout and de Vries, 2016). The statistical description of wind speed is long-standing and well established, as reviewed e.g. by Carta et al. (2009). Conversely only recently the Authors proposed the statistical description of threshold shear velocity (e.g. Raffaele et al., 2016). The cited paper substantially contributes to the background of the present study. It includes a comprehensive review on the uncertainties that affects both experimental measurements and modelling of u_{*t}. In the light of this, a statistical modelling is developed, based on advanced copula-based quantile regression. Joint probability density functions of the sand grain diameter and u_{*t} are derived, as well as the conditional probability density functions of the threshold shear velocity for given values of the diameter.

Both the engineering design needs and the shortcomings of the SD-WA approach pave the way for the probabilistic description of the incoming sand drift. According to the Authors, it can be regarded as equivalent to other environmental actions, in analogy to wind action. Hence, let us briefly outline in the following to which extent the incoming wind speed U is analogous to the sand transport rate Q and to the drift potential DP. First, in wind engineering the wind speed is defined in probabilistic terms due to the uncertainty related to inborn wind variability only. The probabilistic representation of sand transport rate is recommended a fortiori and it is more difficult at the same time, since it is affected by more uncertainties. The variability of both wind and sand features should be taken into account. Second, most of the wind effects on structures, e.g. equivalent static loads or flutter, are related to extreme values of the incoming wind speed. Conversely, windblown sand effects on civil structures are mainly induced by the cumulated values of current values of Q over time, that is DP. In this perspective, windblown sand effects and related assessment recall wind-induced fatigue. In spite of this analogy, some differences remain. Only a few incoming wind directions are considered in directional wind-induced fatigue assessment (see e.g. Repetto and Solari, 2004), i.e. the

ones that induce the highest stresses on the cross section. Conversely, all incoming wind directions are taken into account in assessing the windblown sand drift, since they all contribute in RDP definition.

Bearing the above analogy in mind, three main questions may rise to the Authors' mind: i. How does the uncertainty of both threshold shear velocity and mean wind velocity jointly propagate to RDP? ii. Does the probability distribution of RDP change significantly form a site to another in the same region? iii. Does the gap between characteristic and mean value of RDP make the approach of interest for engineering practice?

The present study aims at contributing in shedding some light on such issues. A general probabilistic approach is proposed and applied to real world sites in Arabian Peninsula. Each site is characterized by its actual wind field and sand granulometry. In particular, variability of both sand characteristics at microscopic scale (comprehensively reflected by threshold shear velocity) and wind speed (i.e. wind direction and intensity) are considered. Other sources of uncertainties reviewed above are not included because the lack of their statistical description. As a result, instead of a single pair of values describing mean RDP magnitude and direction, their probability distributions are obtained. Characteristic values are derived from them, and design values can be derived in turn towards a semi-probabilistic approach. The paper develops accordingly to the above objectives through the following sections. In Section 2, the proposed probabilistic approach is outlined. In Section 3, results referred to some chosen Sites in Arabian Peninsula are shown, compared and discussed. In Section 4, conclusions and perspectives are outlined.

2. Methods

In the following, the proposed probabilistic approach based on the general framework of Fryberger and Dean (1979) is outlined. First, the framework proposed by Fryberger and Dean (1979) is recalled. Then, the proposed probabilistic approach to assess sand drift is shown step-by-step.

Fryberger and Dean (1979) define the directional drift potential and the resultant drift potential on the basis of the model proposed by Lettau and Lettau (1978), where the sand transport rate Q_θ in a given direction θ is expressed as

$$
\begin{aligned}
Q_\theta &= 6.7 \sqrt{\frac{d}{d_r}} \frac{\rho_a}{g} u_{*,\theta}^3 \left(1 - \frac{u_{*t}}{u_{*,\theta}}\right) && \text{if} \quad u_{*,\theta} > u_{*t} \\
Q_\theta &= 0 && \text{if} \quad u_{*,\theta} \le u_{*t},
\end{aligned}
\tag{1}
$$

being d the sand grain diameter, $d_r = 0.25$ mm the reference sand grain diameter, ρ_a the air density, g the gravitational acceleration, u_{*t} the threshold shear velocity and $u_{*,\theta}$ the shear velocity in the corresponding wind direction.

The directional drift potential D_θ (i.e. DP in Fryberger and Dean, 1979, notation) is rephrased as

$$
D_\theta = \frac{1}{\rho_b} \frac{T}{T_r} \sum_{i=1}^{N_\theta} Q_{\theta,i} \Delta t = \frac{T}{T_r} \sum_{i=1}^{N_\theta} D_{\theta,\Delta t,i} \quad (\text{or } D_\theta = 0 \text{ if } N_\theta = 0),
\tag{2}
$$

where ρ_b is the packed bulk sand density, T is the reference time and T_r is the recording time set as a multiple of T. Δt is the sampling interval of the wind speed, not necessarily equal to the 10-minute averaging time, for the sake of generality. The drift potential over the sampling interval $D_{\theta,\Delta t}$ $[m^3 m^{-1} \Delta t^{-1}]$ is estimated postulating Q_θ $[Kg \ m^{-1} s^{-1}]$ constant over Δt.

N_θ follows as the number of occurrences in the reference time in which the wind will blow in the direction θ, and it is expressed as

$$
N_\theta = \frac{T}{T_r} \frac{T_\theta}{\Delta t}, \qquad \text{constrained by} \qquad \sum_{\theta=1}^{2\pi/\Delta\theta} N_\theta + N_0 = N,
\tag{3}
$$

where T_θ is the time over which the wind blows in the direction θ, $\Delta\theta$ is the sector width on which the wind is recorded, N_0 and N are the number of occurrences of calm wind and the number of total occurrences in the reference time T, respectively.

Finally, the resultant drift potential R (i.e. RDP in Fryberger and Dean, 1979, notation) can be easily obtained from the vector sum of D_θ:

$$
R = \sum_{\theta=1}^{2\pi/\Delta\theta} D_\theta.
\tag{4}
$$

3

In the following, resultant drift potential magnitude and direction are defined as $|R|$ and $\hat{R}$, respectively.

It may be useful to highlight that Fryberger and Dean (1979) provide also an index of the directional variability of windblown sand drift, i.e. the ratio between the resultant drift potential magnitude and the sum of drift potential modulus:

$$R/D = \frac{|R|}{\sum_{\theta=1}^{2\pi/\Delta\theta} |D_\theta|}. \qquad (5)$$

In particular, the lower the ratio, the higher the directional variability.

In the proposed probabilistic approach the input quantities u_{*t} and $u_{*,\theta}$ are random variables. Hence, the Fryberger and Dean (1979) framework has to be adapted in order to deal with such random variables. Let us call such approach as Sand Wind Probabilistic (SWP). The steps followed in SWP approach are sketched in the flow chart in Figure 1 and described in the following.
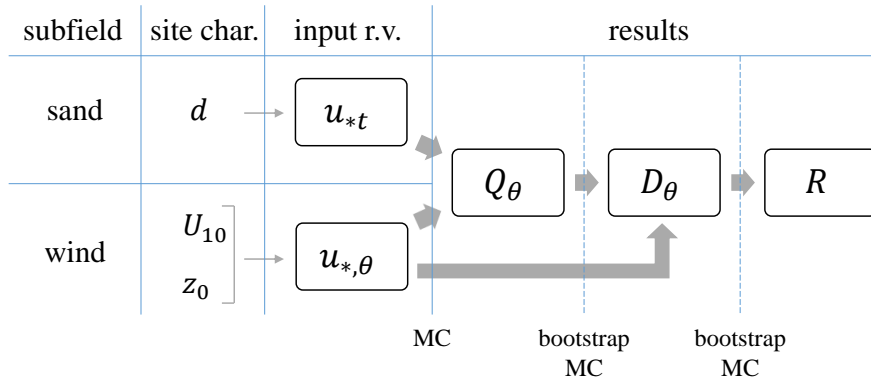

Figure 1: Flow chart of the proposed SWP approach

The site characteristics are needed as input data, with respect to both sand subfield (mean sand diameter d) and wind subfield (aerodynamic roughness z_0 and time series of 10-minute averaged wind speed $U_{10}(t)$). The input random variables u_{*t} and $u_{*,\theta}$ are described from the probability density functions $f(u_{*t})$ and $f(u_{*,\theta})$, respectively. To the Authors' best knowledge, there are no experimental evidence or systematic studies in literature about a dependence between $u_{*,\theta}$ and u_{*t}. In this study, the directional shear velocity and the threshold shear velocity are considered independent random variables. Indeed, u_{*t} depends entirely on the sand characteristics, while $u_{*,\theta}$ depends only on the wind velocity for a given z_0. $f(u_{*,\theta})$ is simply obtained by rescaling the probability density function $f(U_{10,\theta})$, being $u_{*,\theta} = 0.41 U_{10,\theta}/ln(z/z_0)$. Hence, Weibull-type $f(u_{*,\theta})$ results. The conditional probability density functions $f(u_{*t} \mid d)$ are obtained in Raffaele et al. (2016). Interested readers can refer to the paper above for further details. Here, Figure 2 is limited to summarize the final finding of that study, i.e. the statistical description of the threshold shear velocity versus mean sand diameter d by means of some percentiles and statistical moments: the mean value $\mu(u_{*t})$ and 1st, 5th, 25th, 75th, 95th and 99th percentiles p(u_{*t}).

The sand transport rate model proposed by Lettau and Lettau (1978) is adopted because it is widespread in scientific and technical literature (e.g. Fryberger and Dean, 1979; Al-Awadhi and Al-Awadhi, 2009; Barchyn and Hugenholtz, 2011; Yang et al., 2014; Liu et al., 2015), and judged performing better than other sand transport models (Sherman et al., 2013). Q_θ results from the transformation of the continuous random variables $u_{*,\theta}$ and u_{*t}. Q_θ is expected to be a mixed random variable. In fact, Q_θ is characterized by a discrete part, i.e. $Q_\theta = 0$, and a continuous part, i.e. $Q_\theta > 0$, because of the nature of the adopted sand transport rate model (Eq. 1).

Analytically, given the independent random variables $u_{*,\theta}$ and u_{*t}, the probability density function $f(Q_\theta)$ for a given value of d can be evaluated by differentiating its distribution function $F(Q_\theta)$, which, for $q \geq 0$ and $u_{*,\theta} > u_{*t}$, can be
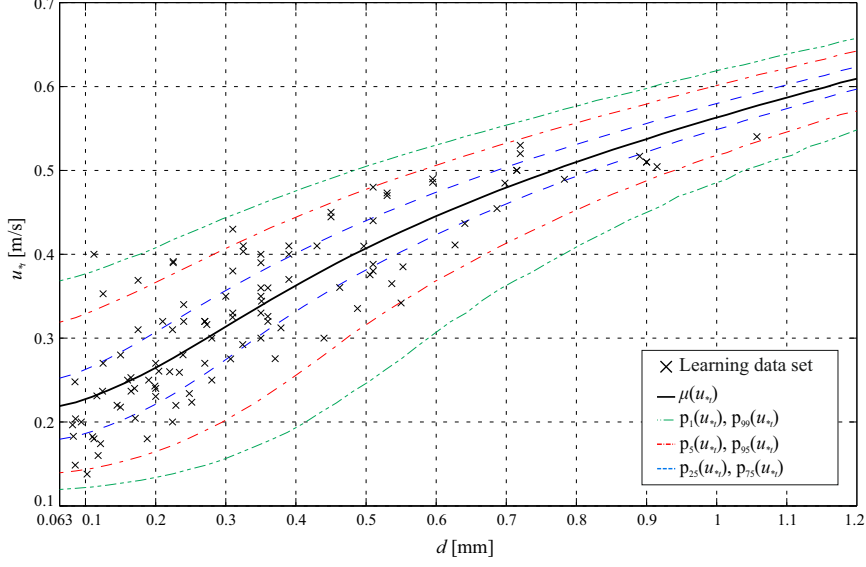
Figure 2: Threshold shear velocity statistics. Mean values $\mu(u_{*t})$ and percentiles $p_1(u_{*t})$, $p_5(u_{*t})$, $p_{25}(u_{*t})$, $p_{75}(u_{*t})$, $p_{95}(u_{*t})$, $p_{99}(u_{*t})$

expressed as

$$
\begin{aligned}
F_{Q_\theta}(q) = P[Q_\theta \leq q] = \quad & P\left[\left\{6.7\sqrt{\frac{d}{d_r}}\frac{\rho_a}{g}u_{*,\theta}^3\left(1 - \frac{u_{*t}}{u_{*,\theta}}\right) \leq q\right\} \bigcap \{u_{*,\theta} > u_{*t}\}\right] \\
= \quad & \int\int_{\left\{(v_1,v_2)\,:\,v_1>v_2;\; v_1^3\left(1-\frac{v_2}{v_1}\right) \leq \frac{q}{6.7}\sqrt{\frac{d_r}{d}}\frac{g}{\rho_a}\right\}} f_{(u_{*,\theta},u_{*t})}(v_1,v_2)dv_1 dv_2 \\
= \quad & \int_0^\infty\left[\int_{v_1-\frac{1}{v_1^2}\frac{q}{6.7}\sqrt{\frac{d_r}{d}}\frac{g}{\rho_a}}^{v_1} f_{(u_{*,\theta},u_{*t})}(v_1,v_2)dv_2\right]dv_1 \\
= \quad & \int_0^\infty\left(F_{u_{*t}}(v_1) - F_{u_{*t}}\left(v_1 - \frac{1}{v_1^2}\frac{q}{6.7}\sqrt{\frac{d_r}{d}}\frac{g}{\rho_a}\right)\right)f_{u_{*,\theta}}(v_1)dv_1.
\end{aligned}
\tag{6}
$$

However, apart for the untractable analytical solution of this double integration, $f(Q_\theta)$ cannot be expressed in explicit form because $f(u_{*t} \mid d)$ is given by a non-parametric kernel density function (Raffaele et al., 2016).

Numerically, Monte Carlo (MC) simulations can be applied (Caflisch, 1998). This approach presents three substantial advantages. First, MC convergence is independent from the number of random variables involved. In fact, it converges with a rate equal to $1/\sqrt{m}$, where m is the number of realizations, regardless of the number to random variables. Second, the very low cost of each single numerical realization of Q_θ allows to perform a large number of realizations for each wind direction. Finally, MC allows to describe the mixed random variable Q_θ in a straightforward manner.

It is worth pointing out that N_θ (Eq. 3) is a random quantity because T_θ is. For this reason, the probability distribution of the directional drift potential $g(D_\theta)$ should be expressed as a mixture of convolutions

$$
g(D_\theta) = \sum_{n=1}^\infty (f_1 * \ldots * f_i * \ldots * f_n)(D_{\theta,\Delta t}) P[N_\theta = n] \quad \text{with} \quad f_i = f \quad \text{for} \quad i = 1,\ldots,N_\theta,
\tag{7}
$$

whose corresponding mean μ and variance σ^2 are

$$
\begin{aligned}
\mu(D_\theta) &= \mu(N_\theta)\,\mu(D_{\theta,\Delta t}) \\
\sigma^2(D_\theta) &= \mu(N_\theta)\,\sigma^2(D_{\theta,\Delta t}) + \mu^2(D_{\theta,\Delta t})\,\sigma^2(N_\theta).
\end{aligned}
\tag{8}
$$

5

In particular, the variance results from the sum of two terms, the first due to the variance of $D_{\theta,\Delta t}$ and the second to the variance of N_θ. It should be pointed out that adoption of a non-random N_θ implies an underestimation of the uncertainty of D_θ, being in this case $\sigma^2(N_\theta) = 0$. It should be also observed that the constraint on the whole set $\{N_\theta, \ \theta = 1, 2, \ldots, n\}$ (see Eq. 3) induces a negative dependence between the variables N_θ, and consequently in the set $\{D_\theta, \ \theta = 1, 2, \ldots, n\}$, which plays a key role in the final distribution of R. Unfortunately, the description of such an effect of the dependence between the variables N_θ can not be provided in a simple and tractable analytical manner. For these reasons, a Monte Carlo approach, based on bootstrapping techniques (Efron and Tibshirani, 1993) from the data set of observed values to generate samples, has been adopted. For each simulation, first the vector $N = (N_1, N_2, \ldots, N_n)$ of registered occurrences of wind in the considered directions has been obtained from the data set. Then, for each direction $\{\theta = 1, 2, \ldots, n\}$, a sample of cardinality N_θ of realizations of $D_{\theta,\Delta t}$ has been randomly chosen. Finally, the matrix $\boldsymbol{D} = (D_1, D_2, \ldots, D_n)$ has been simulated through

$$
\boldsymbol{D} = \begin{bmatrix} D_1 \\ D_2 \\ \vdots \\ D_\theta \\ \vdots \\ D_n \end{bmatrix} = \begin{bmatrix} \sum_{i=1}^{N_1} D_{1,\Delta t,i} \\ \sum_{i=1}^{N_2} D_{2,\Delta t,i} \\ \vdots \\ \sum_{i=1}^{N_\theta} D_{\theta,\Delta t,i} \\ \vdots \\ \sum_{i=1}^{N_n} D_{n,\Delta t,i} \end{bmatrix},
\tag{9}
$$

where any $D_{\theta,\Delta t,i}$ is a realization of $D_{\theta,\Delta t}$ previously extracted from the data set.

Analytically, R is the vector sum of the components D_θ of the matrix $\boldsymbol{D}$ (Eq. 4), thus a realization of the resultant drift potential R can be immediately assessed once the realization of $\boldsymbol{D}$ is given. A set of numerical realizations of R can be computed by repeating the same procedure multiple times, and the distribution of R can be estimated through such a sample.

3. Applications and results

In the following, the proposed SWP approach is applied to five Sites located in the Arabian Peninsula. In Subsection 3.1, the layout of the study is shown. Geographical location and aeolian sand grain size of the chosen sites are reported. In Subsection 3.2, SWP approach is applied to Site 1. Obtained results are shown in terms of both intermediate, i.e. Q_θ and D_θ, and final, i.e. R, results in order to follow and comment step-by-step the full adopted procedure. Finally, in Subsection 3.3, final results from Sites 1-5 sites are summarized and compared.

3.1. Study layout

The site selection obeys to three criteria. Sites with a complete enough anemometric database are first retained. Among them, sites are selected to sample the huge variability of both sand and wind subfields in Arabian Peninsula. Finally, sites are chosen in reason of their proximity to railway lines having in mind the vulnerability of such infrastructures to windblown sand.

In Figure 3, Sites 1-5 are represented on Arabian Peninsula (blue dots). On the same Figure, some operating/under construction/planned railway tracks are sketched. In particular, the 950 km long Saudi Landbridge links Jeddah with the Saudi Arabia capital Riyadh. The 2750 km North South Railway Line links northern Saudi Arabia with Riyadh and the port city Ras Al-Khair. The 450 km long Haramain High Speed Rail links the cities of Medina and Mecca. Ethiad Rail is part of the United Arab Emirates' national 1200 km railway network.

Sites coordinates and mean sand grain size d are reported in Table 1. Mean grain sizes are derived from sedimentology studies of arabian sand dunes (Al-Sari and Uddin, 1981; Ehlen, 1993; Al-Harthi, 2002; Edgell, 2006). In particular, Sites 1, 3 and 4 are sensitive to the sand of Ad Dahna desert, made of medium grained, well sorted quartz sand. Site 2 is sensitive to the sand of Jeddah plain. Site 5 is sensitive to the fine grained, moderately well sorted sand of Rub' al Khali desert.

The aerodynamic roughness is set equal to $z_0 = 4e{-}3$ m in all Sites. The wind velocity dataset refers to $T_r = 5$ years from January 2008 to December 2012 for all stations as well. The 10-min average wind direction is measured in the horizontal plane with a sampling interval $\Delta\theta = 10°$ at all the selected anemometric stations. $n = 36$ directions
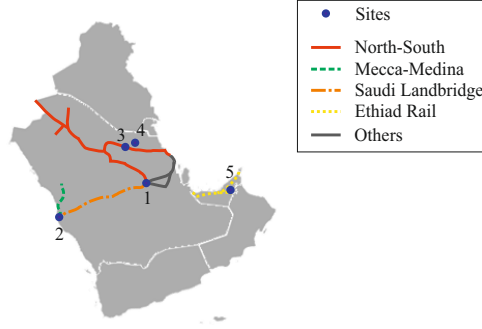
Figure 3: Sketch of the selected sites (blue dots) and railways tracks (lines)

Table 1: Sites of incoming sand drift estimation

Site number	Site name	Latitude	Longitude	d [mm]
1	Riyad	24°4'1.20"N	47°34'58.80"E	0.35
2	Jeddah	21°41'60.00"N	39°10'58.80"E	0.25
3	Hafr Al-Batin	27°55'1.20"N	45°31'1.20"E	0.30
4	Al Qaisumah	28°19'1.20"N	46°7'58.80"E	0.30
5	Al Ain	24°12'2.99"N	55°45'40.00"E	0.16

result. The 10-min average wind velocity is recorded with a sampling interval in time $\Delta t = 1$ hour at all the anemometric stations (sampling rate 24/144). The actually available datasets at the selected anemometric stations include missing data due to anemometric breakdowns and/or operational problems. Missing data are in average equal to 4% of the complete dataset. They are evaluated to be almost uniformly distributed along the day. Both the sampling rate and missing data are sources of incompleteness of the dataset. In literature (see e.g. Burlando et al., 2013) is widely accepted that randomly distributed data incompleteness is usually not influential on the probability distribution of the 10-min average wind velocity, while it may lead to underestimations of the extreme values. It is worth recalling that windblown sand drift potential R is mainly induced by the cumulated values of current values of Q over time, resulting from the 10-min average wind velocity in turn. Hence, data incompleteness is not expected to affect the obtained results. Finally, the resultant drift potential R is expressed over a reference time $T = 1$ year.

The results discussed in the next Subsections are obtained by MC approach. Hence, results convergence should be discussed every time a random variable is introduced and numerically generated. Convergence is classically evaluated by referring to weighted residuals of the first statistical moments of each random variable. The cardinality of the set of realizations for each random variable is chosen in order to reach a weighted residual lower or at least equal to $1e-2$. In the following, the cardinality of each random variable is reported for the sake of completeness, while convergence studies are not reported for the sake of brevity.

3.2. Results for site 1

The characteristics of the in-situ sand subfield is summarized by $d = 0.35\,mm$ (Table 1). The related input random variable is the threshold shear velocity. Its probability density function $f(u_{*t}|d = 0.35\,mm)$ is derived from Raffaele et al. (2016). Related u_{*t} statistics are reported in Table 2 in terms of mean value μ, standard deviation σ and coefficient of variation *c.o.v.* It is worth recalling that $f(u_{*t}|d)$ is the same in each wind direction, since it depends solely on sand characteristics.

The wind subfield is obtained by mean wind speed in-situ measurements. U_{10} variability is assessed in terms of both *non-directional* and *directional* statistics.

Non-directional statistics is summarized in Figure 4. U_{10} time history is shown in Figure 4(a). Both mean wind speed

7

$\mu(U_{10})$ and mean threshold velocity $\mu(U_t)$ are plotted on the same graph. U_{10} variability is described by the Hybrid Weibull (HW) model (Takle and Brown, 1978). HW probability density function $f(U_{10})$ is defined as follows:

$$f_{(\lambda,k)}(U_{10}) = \begin{cases} F_0 & \text{for } U_{10} = 0 \\ (1 - F_0) \dfrac{k}{\lambda} \left(\dfrac{U_{10}}{\lambda}\right)^{k-1} e^{-U_{10}/\lambda^k} & \text{for } U_{10} > 0 \end{cases} \tag{10}$$

where F_0 is the rate of zero values, i.e. the frequency of calm wind, k is the shape parameter and λ is the scale parameter. HW $f(U_{10})$ is plotted in Figure 4(b).
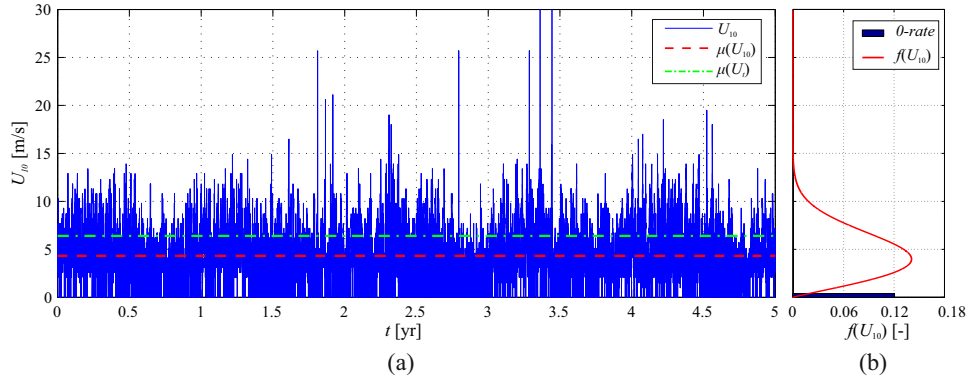

Figure 4: Site 1. Non-directional statistics of mean wind speed: Wind time history (a) and Hybrid Weibull fitting (b)

Wind shear velocity is recovered from mean wind speed in-situ measurement. HW $f(U_{10})$ is rescaled into HW $f(u_*)$. u_* statistical parameters and moments are reported in Table 2, where they can be compared with u_{*t} ones. In particular, the threshold shear velocity is higher than the shear velocity in mean terms, while the highest variability is addressed to the wind subfield.

Table 2: Site 1. Statistical parameters and moments of the non-parametric $f(u_{*t}|d = 0.35\ mm)$ and Hybrid Weibull $f(u_*)$

Random variable	F_0 [−]	k [−]	λ [$m\ s^{-1}$]	μ [$m\ s^{-1}$]	σ [$m\ s^{-1}$]	$c.o.v.$ [−]
u_{*t}	-	-	-	0.34	0.06	0.18
u_*	0.12	2.09	0.29	0.25	0.13	0.50

Directional statistics is shown by means of the wind rose and the polar diagram in Figure 5. Calm wind, i.e. $U_{10,\theta}$ null values, is filtered since it is non-directional by nature and does not contribute in defining directional statistics. Figure 5(a) shows a very broad wind directionality. However, North and South-SouthEast are the directions having the highest occurrence frequency. In Figure 5(b), the empirical probability density function of the wind speed in North direction is shown as an example. Figure 5(c) depicts the variation of probability density function of both wind speed $U_{10,\theta}$ and erosion threshold U_t by means of their directional mean values values and extreme percentiles (i.e. 5th percentile p_5 and 95th percentile p_{95}), as a function of wind direction $\theta = 1, \ldots, n$. $\mu(U_t)$ is higher than $\mu(U_{10,\theta})$ for every direction, but the 95th percentile of the wind speed $p_{95}(U_{10,\theta})$ overcomes the corresponding percentile of the threshold velocity $p_{95}(U_t)$ for winds blowing from around North and from South-SouthWest.

$U_{10,\theta}$ is converted into $u_{*,\theta}$ dataset. Classic Weibull probability density function $f(u_{*,\theta})$ are fitted for each direction. Numerical realizations of u_{*t} and $u_{*,\theta}$, consistent with $f(u_{*t})$ and $f(u_{*,\theta})$ respectively, are generated in order evaluate the sand transport rate Q within MC approach. u_{*t} and $u_{*,\theta}$ cardinality $\# = 1e+6$ is adopted for each direction. Sand transport rate results are organized in the form of sand rose in Figure 6(a) in analogy with the wind rose in Figure 5(a). In fact, the length of each bin is the same in both roses. The wind rose and the sand rose have the same direction frequencies. Hence, the relative length of each bin is the same in both roses. This is due to the fact that one
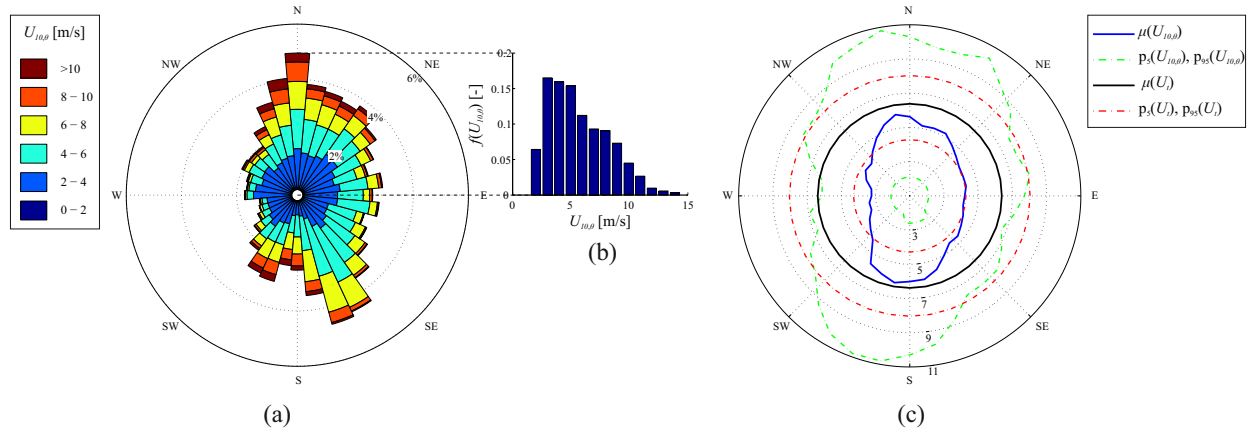
Figure 5: Site 1. Directional statistics of mean wind speed: wind rose (a), empirical probability density function of the wind speed in North direction (b), polar diagram of U_{10} and U_t statistics (c)

realization of Q for a given direction results from the corresponding realization of U_{10} along the same direction θ. Conversely, the probability density function $f(Q_\theta)$ for each direction does not result from a simple rescaling of the corresponding $f(u_{*,\theta})$, because of the piece-wise, non-linear transformation (Eq. 1). In particular, for $0 < u_{*,\theta} < u_{*t}$, $Q_\theta = 0$ even if this does not correspond to wind calm conditions. Hence, the color pattern in each bin significantly varies. An example is explicitly given by the empirical probability density functions for North direction (Fig. 5-b and 6-b). Figure 6(c) depicts the mean value and the 95th percentile of the sand transport rate as a function of θ. $\mu(Q_\theta)$ and $p_{95}(Q_\theta)$ are higher for winds blowing from around North and from South-SouthWest, that are the direction for which $p_{95}(U_{10,\theta}) > p_{95}(U_t)$ (see Fig.5-c).
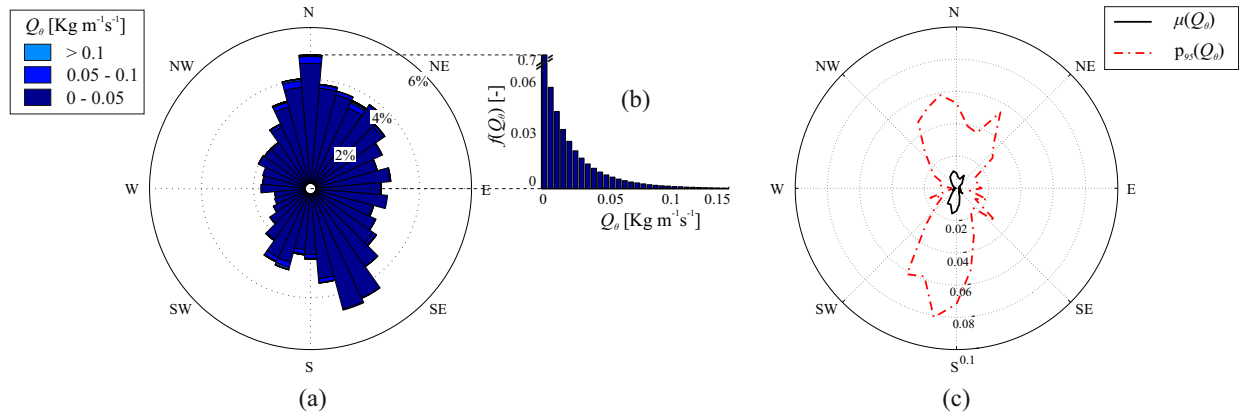

Figure 6: Site 1. Sand transport rate statistics: sand transport rate rose (a), sand transport rate empirical probability density function in North direction (b), polar diagram of sand transport rate statistics (c)

The following remarks can be outlined. First, the distribution is no longer a continuous distribution: its hybrid nature is due to the first part of the piece-wise transformation, i.e. $Q_\theta = 0$ if $u_{*,\theta} \leq u_{*t}$. Second, the distribution is no longer a Weibull-type one, due to the non-linear transformation. In particular, distributions are strongly right-sided skewed. Finally, the sand transport rate directional statistics are strongly bimodal, with North and South prevailing directions, in contrast with the very broad wind directionality (Fig.5-a). This is due to the fact that the sand transport rate Q_θ depends on the cube of the effective shear velocity $u_{*,\theta,eff}^3 = u_{*,\theta}^3 - u_{*,\theta}^2 u_{*t}$. Referring to Figure 5(c), low-speed winds from West and East do not contribute to Q_θ, while high-speed winds from North and South almost solely contribute

to Q_θ.

The drift potential over the sampling interval $D_{\theta,\Delta t}$ $[m^3\ m^{-1} hr^{-1}]$ is simply obtained from Q_θ $[Kg\ m^{-1} s^{-1}]$ considering the packed bulk sand density $\rho_b = 1.8e{+}3\ kg\ m^{-3}$.

The number of occurrences N_θ is assessed by bootstrapping a sample of cardinality $N = 8768$ (i.e. the number of Δt in T) from the actual wind velocity dataset. The wind direction frequencies N_θ/N are shown by box plots in Figure 7(a). On the same graph, calm wind frequency is plotted too. It should be highlighted that the influence of calm wind on D_θ is taken into account by N_θ. In fact, wind direction frequencies are computed considering the frequency of calm wind (see Eq.3).

Once $D_{\theta,\Delta t}$ and N_θ are assessed over each direction, the drift potentials D_θ over $T = 1$ year are obtained following Equation 9. In particular, Equation 9 is applied by bootstrapping a sample of $D_{\theta,\Delta t}$ and N_θ realizations, both having cardinality $\# = 1e{+}5$. The same cardinality $\#_{D_\theta}$ for each D_θ follows from MC. In Figure 7(b), drift potential mean values and percentiles are plotted as a function of θ to summarize directional statistics and related $f(D_\theta)$. The non-parametric probability density function $f(D_\theta)$ which describes the incoming sand drift from North in $T = 1$ year, is shown in Figure 7(c) by way of example.
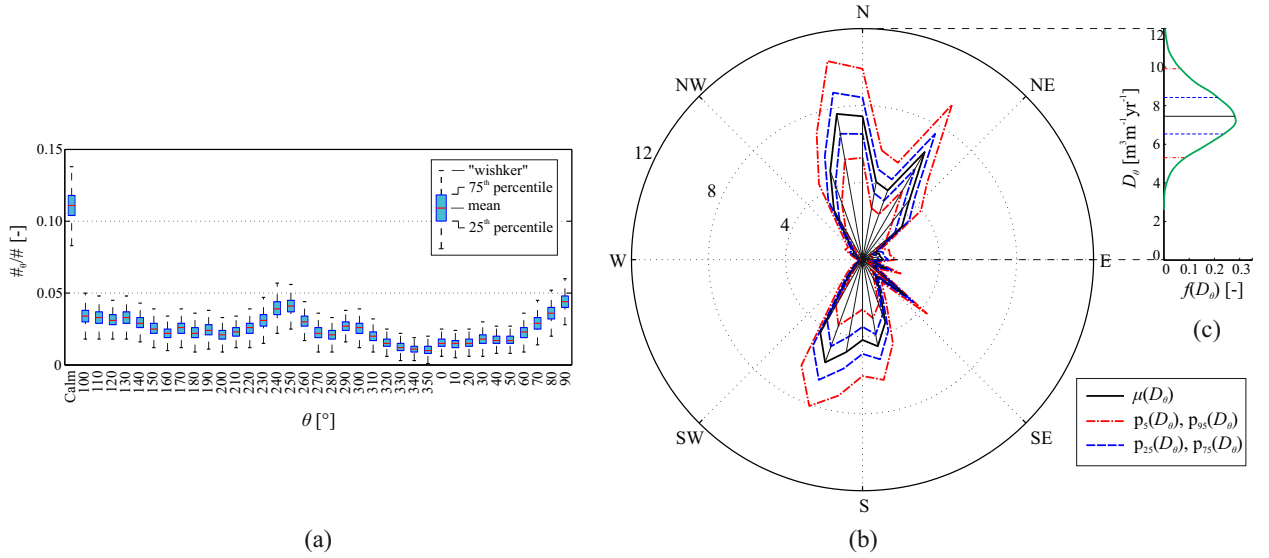

Figure 7: Site 1. Wind direction frequencies by N_θ/N box plot (a). Drift potential D_θ directional statistics (b), drift potential probability density function in North direction (c).

Three remarks follow. First, N_θ variability is low, at least for this site. Hence, the variance of D_θ is mainly due to the variance of $D_{\theta,\Delta t}$, while the variance of N_θ is relatively small (see Eq.8). Second, the drift potential directional statistics are strongly bimodal with North and South prevailing directions in accordance with the sand transport rate ones (see Fig.6-c). Finally, the cumulative sum of the very skewed $f(Q_\theta)$ gives rise to almost symmetric $f(D_\theta)$. This is compliant to the central limit theorem: the sum of independent random variables tends to a normally distributed random variable even if the original random variables are not.

Figure 8 provides a synopsis of the uncertainty propagation from erosion threshold and wind speed to sand transport rate and drift potential. The coefficient of variation and skewness modulus of these random variables are plotted as a function of the direction θ in Figures 8 (a) and (b), respectively. The $c.o.v.$ of the input random variables $(U_{10,\theta}, U_t)$ is relatively small ($c.o.v. \approx 1e{-}0.5$). Uncertainty is magnified by an order of magnitude proceeding to Q_θ ($c.o.v. \approx 1e{+}0.5$), while $c.o.v.$ is damped again passing from Q_θ to D_θ ($c.o.v. \approx 1e{-}0.5$). Indeed, on the one hand, transformation of random variables done in order to assess Q (i.e. Eq.1) magnifies the uncertainty of the initial random variables $U_{10,\theta}$ and U_t. On the other hand, the random sum of identically and independent distributed random variables (Eq.9) damps $c.o.v.$. The $c.o.v.$ of the random variables above shows slight differences over θ. U_t does not depend on θ at all, $c.o.v.(U_{10,\theta})$ is almost constant for this site, $c.o.v.(Q_\theta)$ and $c.o.v.(D_\theta)$ in turn are higher for winds

blowing from East and West, i.e. the less frequent wind directions. The skewness modulus shows approximately the same behavior of *c.o.v.* $|sk(Q_\theta)|$ increases significantly with respect to $|sk(U_t)|$ and $|sk(U_{10,\theta})|$, while $|sk(D_\theta)|$ decreases again. In particular, $|sk(D_\theta)|$ is lower for winds blowing from around North and South directions.
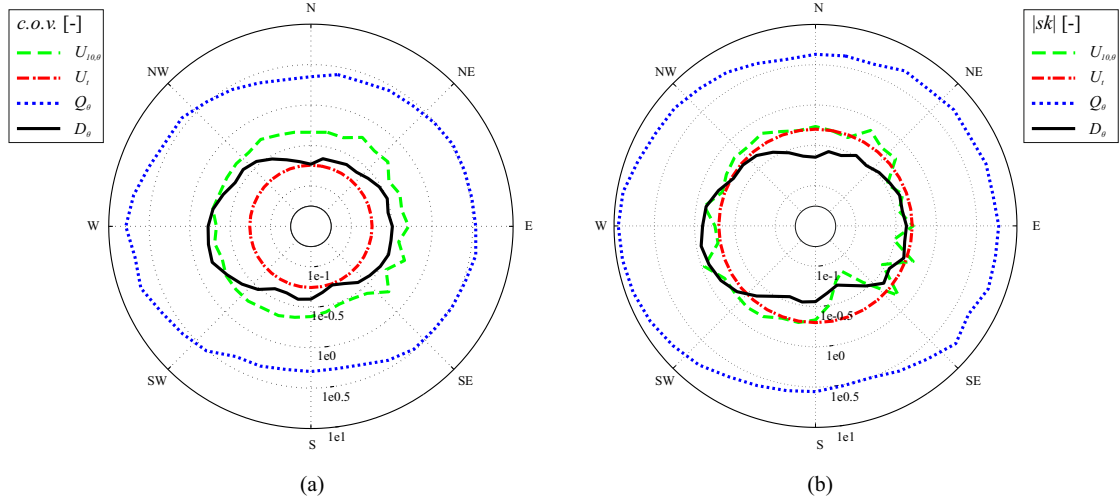

Figure 8: Site 1. Uncertainty propagation from U_{10} and U_t to Q_θ and D_θ in terms of polar diagrams of coefficient of variation (a) and skewness (b)

Finally, in Figure 9(a), each black dot represents a single realization the resultant drift potential *R*. The radial coordinate of the dots is the vector magnitude $|R|$, while the angular coordinate is the vector direction $\hat{R}$. Each realization of *R* is numerically obtained from one realization of ***D*** through Equations 4 and 9 by bootstrapping (Efron and Tibshirani, 1993). The ensemble of black dots graphically visualizes the whole set of numerical realizations of *R*. The cardinality of *R* is $\#_R = 5e+4$. In the following we call "realization cloud" the ensemble of black dots. The mean resultant drift potential vector $\mu(R)$ is depicted by the red arrow on the same graph. *R* can be described in probabilistic terms by the joint probability density function $f(|R|, \hat{R})$ of the two random variables $|R|$ and $\hat{R}$. $f(|R|)$ and $f(\hat{R})$ marginal densities are shown in Figure 9(b) and (c), respectively.

The realization cloud appears to be comma-shaped in circular coordinates, i.e. tear-shaped in cartesian coordinates. This shape indicates a significant skewness of $\hat{R}$, as testified by its marginal distribution. The radial width of the realization cloud provides a qualitative graphical reading of the variability of *R* magnitude. The circumferential extent of the cloud qualitatively describe the variability of *R* direction. For this site, the variability of $\hat{R}$ is by far higher than the one of $|R|$. This is confirmed by the marginal distributions in Figures 9(b) and (c). From a qualitative point of view, it is worth pointing out that the only mean value (red arrow) is a poor description of the sand drift phenomenon. Conversely, realization cloud and related high-order statistics provide a more complete description. In general, SD-WA approach loses fundamental information of *R*, while the proposed SWP approach provides complete statistics. The quantitative statistics of *R* for this Site and all remaining Sites are reported in the following Subsection.

3.3. Comparative analysis Sites 1-5

In the following, all the selected Sites are accounted for. Both wind and windblown sand fields are probabilistically evaluated and critically compared.

In Figure 10, U_{10} wind roses and polar diagrams of resultant drift potential *R* are represented on Arabian Peninsula map. Realization clouds of the resultant drift potential and marginal densities are plotted as well. On the same graphs, the mean values of *R* are reported (red arrows). In short, Figure 10 collects the results of the initial and final step of the proposed procedure. Wind rose shape testifies a variety of wind regimes: wide unimodal, i.e. Site 2, acute bimodal, i.e. Site 3, obtuse bimodal, i.e. Sites 1 and 5, complex, Site 4. Realization cloud shape, dimension and density change significantly moving from a site to another. The realization clouds appear to be comma-shaped in polar diagrams (i.e. tear-shaped in cartesian coordinates), or kidney-shaped (i.e. elliptical-shaped in cartesian coordinates). Comma
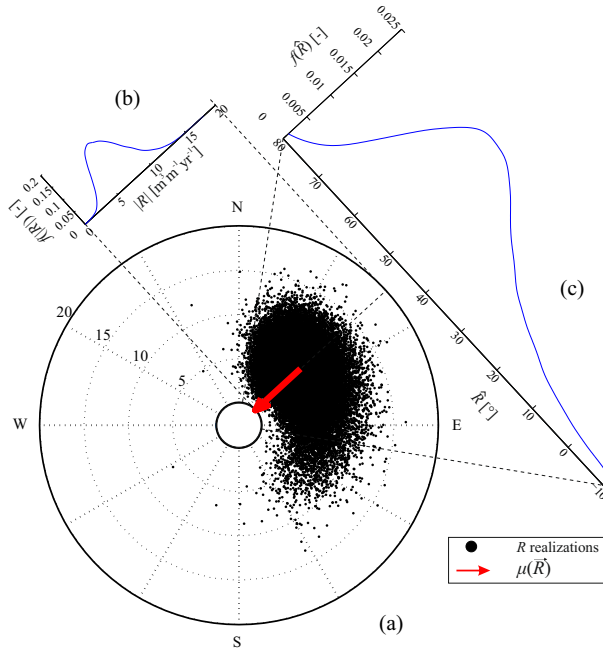
11

Figure 9: Site 1. Resultant drift potential (a), resultant drift potential magnitude marginal density (b) and resultant drift potential direction marginal density (c).

shape (Sites 1 and 5) indicates a significant skewness of $\hat{R}$, while kidney shape (Sites 2,3,4) indicates weakly skewed magnitude and direction. The wider the realization cloud in radial and/or circumferential direction, the higher the variation of R, in magnitude and direction, respectively. Variations of both $|R|$ and $\hat{R}$ are small at Sites 2 and 3, so that kidney-shaped cloud appear as elliptical. Site 4 is remarkably characterized by very high variation of $\hat{R}$ and a small variation of $|R|$. The marginal densities $f(|R|)$ and $f(\hat{R})$ clearly reflect these differences. In particular, while in some cases they recall Gaussian distributions (Sites 2 and 3), in others they appear asymmetric, mainly with respect to the direction ($f(\hat{R})$ at Sites 1 and 5). In general, the relation between wind rose and realization cloud is not straightforward, because of the non-linear relation between U_{10} and Q. Furthermore, wind roses graphically point out wind direction frequencies much more effectively than wind speed frequencies. However, it is worth pointing out that the more complex the wind rose, the wider the realization cloud.

Non-dimensional statistics of both $|R|$ and $\hat{R}$ are reported in Table 3 to summarize the obtained results and quantitatively compare the Sites. Variation and skewness of $|R|$ and $\hat{R}$ are assessed in order to understand how much the random variables are dispersed and how far are from Gaussianity. The variability of $|R|$ is expressed by means of $c.o.v.$, while the variability of $\hat{R}$ is directly expressed by the angular deviation σ. It is worth to point out that since $\hat{R}$ is a circular random variable, circular statistics is assessed (Fisher, 1995; Berens, 2009). The lowest variability is addressed to Site 2, i.e. the Site with unimodal wind regime, while the highest variability is addressed to e.g. Sites 1 and 4, i.e. the Sites with obtuse bimodal or complex wind regimes. Concerning probability density functions symmetry, Sites 1 and 5 show the most skewed distributions, while Site 3 one is almost symmetric.

The design of infrastructures in arid environments should be based on sand drift magnitude related to a low probability of exceedance. Hence, characteristic values (i.e. extreme percentiles) of both R magnitude and direction are included in Table 3. The ratio between 95th percentile and mean value p_{95}/μ is assessed as regards R magnitude. The study gives rise to characteristic values up to ≈ 1.6 times the mean value (Site 1). In other words, the evaluation of $|R|$ in mean terms only significantly underestimates the amount of transported sand. The angular distance $|p_{95} - p_5|$ is evaluated, regarding $\hat{R}$. Both percentiles are referred to anti-clockwise circular direction from East. In other words, $|p_{95} - p_5|$ provides a quantitative measure of the variability of $\hat{R}$ based on characteristics directions. This measure is the well posed probabilistic reading of the estimate of drift direction variability proposed by Fryberger and Dean (1979)
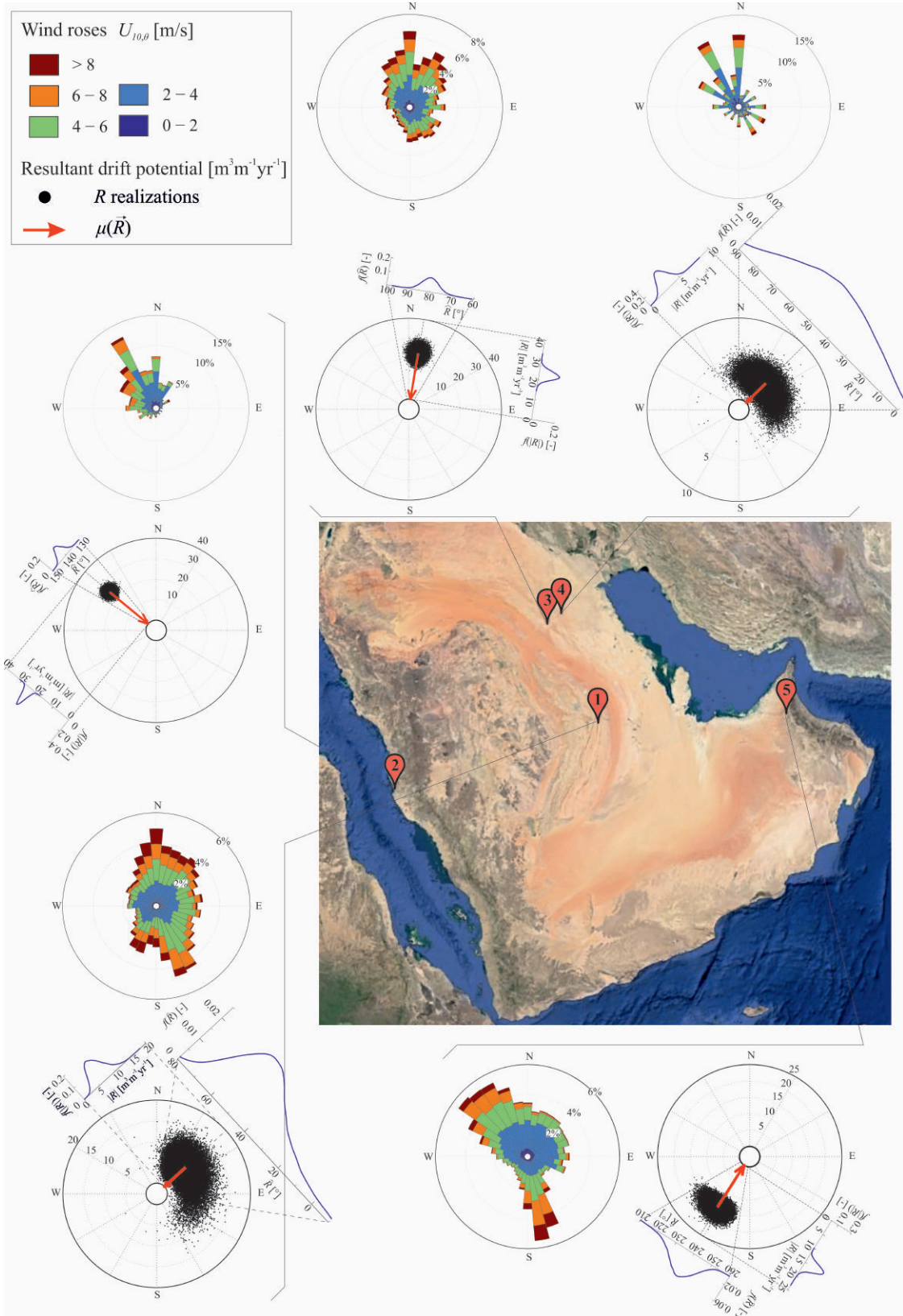
12

Figure 10: Sites 1-5. Wind roses and resultant drift potentials around Arabian Peninsula

in deterministic terms through Equation 5. The highest $|p_{95} - p_5|$ angular distance is observed for Site 4, i.e. $\approx 88°$, while the lowest, $\approx 8°$, is observed for Site 2.

Table 3: Sites 1-5. Statistics of resultant drift potential magnitude and direction

| | $|R|$ $[m^3 m^{-1} yr^{-1}]$ | | | $\hat{R}$ $[°]$ | | |
	$c.o.v.$ $[-]$	sk $[-]$	$p_{95}/\mu [-]$	σ $[°]$	sk $[-]$	$|p_{95} - p_5|[°]$
Site 1	0.32	0.37	1.57	20.77	2.61	77.22
Site 2	0.06	0.02	1.09	2.52	0.38	8.28
Site 3	0.10	0.01	1.16	3.88	-0.05	12.78
Site 4	0.27	0.11	1.46	24.09	0.60	87.80
Site 5	0.10	0.28	1.17	7.11	1.05	23.22

4. Conclusions

The present study introduces a new Sand-Wind Probabilistic (SWP) approach to evaluate incoming windblown sand drift potentials and resultant drift potentials. The approach adapts the general framework proposed by Fryberger and Dean (1979) in order to deal with the sources of uncertainty related to both wind and sand subfields. The input uncertainties on U_{10} and u_{*t} propagate to the final result, i.e. R, passing through the definition of Q_θ and D_θ.

The following concluding remarks can be outlined, bearing in mind the three kickoff questions raised in Introduction. First, uncertainty of both threshold shear velocity and mean wind velocity are magnified passing to the directional sand transport rate Q_θ by about an order of magnitude. Subsequently, uncertainty is damped from Q_θ to the drift potential D_θ, and it is further damped to the resultant drift R. Magnification is due to the cubic dependency of Q versus u_* and u_{*t}, while damping results from cumulating in time and vector summing over directions. Second, the probability distribution of the resultant drift potential changes significantly form a site to another in the same region. Complex wind regimes are particularly prone to cause windblown sand drift with high inborn variability. For instance, the highest $c.o.v.(|R|)$ and $\sigma(\hat{R})$ are referred to sites showing obtuse bimodal or complex wind roses. Changes in the sand granulometry and related shear threshold velocity probability distribution from one site to another also affect R. Finally, the proposed SWP probabilistic approach allows to obtain characteristic values of R, while the Sand Deterministic-Wind Averaged (SD-WA) approach adopted up to now in scientific literature and engineering practice does not provide sufficient statistics to describe correctly the phenomenon. The gap between characteristic and mean value of RDP makes the approach of interest for engineering practice and grounds the semi-probabilistic approach to design of civil infrastructure in arid regions. Regarding sites with complex wind regimes, on the one hand, the characteristic value of $|R|$ is about 1.5 times the mean value. On the other hand, the angular distance between the mean direction and the characteristic values of $\hat{R}$ is about $40°$.

In the light of the obtained results, we suggest four research perspectives. First, the role played by each considered random variable in variability of sand drift should be ascertained by means of a numerical sensitivity study, i.e. by setting a constant grain diameter (and hence the probability density function of u_{*t}) and varying the wind field, and vice versa. Second, the proposed approach needs to be validated by in-situ, long-term, continuous and automatic recording of the sand drift, analogously to wind speed measurements. Traditional sand trap (Nickling and Neuman, 1997; Weaver and Wiggs, 2011) are not adequate to this purpose. Piezoelectric sand flux sensor (Udo, 2009) proved encouraging performances during prototype testing in operational conditions. This technology will enable in the next future years-long site measurements. Third, having in mind the vast amount of sand transport rate models in literature, Q model uncertainty should be investigated and, if significant, incorporated in the adopted probabilistic method. Finally, sand drift extreme values statistics would worth to be described in order to assess how much stand storms weigh on the total amount of the resultant drift potential and on disastrous events.

14

References

Al-Awadhi, J.M., Al-Awadhi, A.A., 2009. Modeling the aeolian sand transport for the desert of Kuwait: Constraints by field observations. Journal of Arid Environments 73, 987–995. doi:10.1016/j.jaridenv.2009.04.023.

Al-Harthi, A., 2002. Geohazard assessment of sand dunes between Jeddah and Al-Lith, western Saudi Arabia. Environmental Geology 42, 360–369. doi:10.1007/s00254-001-0501-z.

Al-Sari, A., Uddin, W., 1981. Eolian sand problem: an engineering evaluation, in: Proceedings Symposium Geotechnical Problems in Saudi Arabia.

Alghamdi, A.A., Al-Kahtani, N.S., 2005. Sand Control Measures and Sand Drift Fences. J. Perform. Constr. Facil. 19, 295–299. doi:10.1061/(ASCE)0887-3828(2005)19:4(295).

Bagnold, R., 1941. The Physics of Blown Sand and Desert Dunes. Methuen. doi:10.1007/978-94-009-5682-7.

Barchyn, T.E., Hugenholtz, C.H., 2011. Comparison of four methods to calculate aeolian sediment transport threshold from field data: Implications for transport prediction and discussion of method evolution. Geomorphology 129, 190–203. doi:10.1016/j.geomorph.2011.01.022.

Barchyn, T.E., Martin, R.L., Kok, J.F., Hugenholtz, C.H., 2014. Fundamental mismatches between measurements and models in aeolian sediment transport prediction: The role of small-scale variability. Aeolian Research 15, 245–251. doi:10.1016/j.aeolia.2014.07.002.

Berens, P., 2009. Circstat: A matlab toolbox for circular statistics. Journal of Statistical Software 31. doi:10.18637/jss.v031.i10.

Bofah, K.K., Al-Hinai, K.G., 1986. Field tests of porous fences in the regime of sand-laden wind. Journal of Wind Engineering and Industrial Aerodynamics 23, 309–319. doi:10.1016/0167-6105(86)90051-6.

Bogle, R., Redsteer, M., Vogel, J., 2015. Field measurement and analysis of climatic factors affecting dune mobility near Grand Falls on the Navajo Nation, southwestern United States. Geomorphology 228, 41–51. doi:10.1016/j.geomorph.2014.08.023.

Burlando, M., De Gaetano, P., Pizzo, M., Repetto, M., Solari, G., Tizzi, M., 2013. Wind climate analysis in complex terrain. Journal of Wind Engineering and Industrial Aerodynamics 123, 349–362. doi:10.1016/j.jweia.2013.09.016.

Caflisch, R., 1998. Monte carlo and quasi-monte carlo methods. Acta Numerica 7, 1–49. doi:10.1017/S0962492900002804.

Carta, J.A., Ramírez, P., Velázquez, S., 2009. A review of wind speed probability distributions used in wind energy analysis: Case studies in the Canary Islands. Renewable and Sustainable Energy Reviews 13, 933–955. doi:10.1016/j.rser.2008.05.005.

Cheng, J., Xue, C., 2014. The sand-damage-prevention engineering system for the railway in the desert region of the Qinghai-Tibet plateau. J. Wind Eng. Ind. Aerodyn. 125, 30–37. doi:10.1016/j.jweia.2013.11.016.

Cheng, J.j., Jiang, F.q., Xue, C.x., Xin, G.w., Li, K.c., Yang, Y.h., 2015. Characteristics of the disastrous wind-sand environment along railways in the Gobi area of Xinjiang, China. Atmospheric Environment 102, 344–354. doi:10.1016/j.atmosenv.2014.12.018.

Dong, Z., Chen, G., He, X., Han, Z., Wang, X., 2004. Controlling blown sand along the highway crossing the Taklimakan Desert. Journal of Arid Environments 57, 329–344. doi:10.1016/j.jaridenv.2002.02.001.

Dong, Z., Liu, X., Wang, H., Wang, X., 2003. Aeolian sand transport: a wind tunnel model. Sediment. Geol. 161, 71–83. doi:10.1016/S0037-0738(03)00396-2.

Duan, S., Cheng, N., Xie, L., 2013. A new statistical model for threshold friction velocity of sand particle motion. Catena 104, 32–38. doi:10.1016/j.catena.2012.04.009.

Edgell, H.S., 2006. Arabian Desert. Springer.

Edwards, B.L., Namikas, S.L., 2015. Characterizing the sediment bed in terms of resistance to motion: Toward an improved model of saltation thresholds for aeolian transport. Aeolian Research 19, 123–128. doi:10.1016/j.aeolia.2015.10.004.

Efron, B., Tibshirani, R., 1993. An Introduction to the Bootstrap. Chapman & Hall/CRC, New York.

Ehlen, J., 1993. Physical Characteristics of Some Solis from the Middle East. Technical Report. U.S. Army Topographic Engineering Center (TEC-0032).

Fisher, N., 1995. Statistical Analysis of Circular Data. Cambridge University Press. doi:https://doi.org/10.1017/CBO9780511564345.

Fryberger, S., Dean, G., 1979. A Study of Global Sand Seas. chapter Dune forms and wind regime. pp. 137–155.

Hoonhout, B.M., de Vries, S., 2016. A process-based model for aeolian sediment transport and spatiotemporal varying sediment availability. Journal of Geophysical Research: Earth Surface 121, 1555–1575. doi:10.1002/2015JF003692.

Iversen, J., White, B., 1982. Saltation threshold on earth, mars and venus. Sedimentology 29, 111–119. doi:10.1111/j.1365-3091.1982.tb01713.x.

Kilibarda, Z., Kilibarda, V., 2016. Seasonal geomorphic processes and rates of sand movement at Mount Baldy dune in Indiana, USA. Aeolian Research 23A, 103–114. doi:10.1016/j.aeolia.2016.10.004.

Kok, J.F., Parteli, E.J.R., Michaels, T.I., Karam, D.B., 2012. The physics of wind-blown sand and dust. Reports on Progress in Physics 75, 106901. doi:10.1088/0034-4885/75/10/106901.

Lancaster, N., Baas, A., 1998. Influence of vegetation cover on sand transport by wind: field studies at Owens Lake, California. Earth Surface Processes and Landforms 23, 69–82. doi:10.1002/(SICI)1096-9837(199801)23:1<69::AID-ESP823>3.0.CO;2-G.

Lettau, K., Lettau, H., 1978. Experimental and micro-meteorological field studies of dune migration. Technical Report 101, 110-147. Exploring the Worlds Driest Climate (IES Report, 101, 110147).

Liu, L., Yang, Y., Shi, P., Zhang, G., Qu, Z., 2015. The role of maximum wind speed in sand-transporting events. Geomorphology 238, 177–186. doi:10.1016/j.geomorph.2015.03.007.

McKenna, N., 2003. Effects of temperature and humidity upon the entrainment of sedimentary perticles by wind. Boundary Layer Meteorol. 108, 61–89. doi:10.1023/A:1023035201953.

McKenna Neuman, C., Nickling, W., 1989. A theoretical and wind tunnel investigation of the effect of capillary water on the entrainment of sediment by wind. Can. J. Soil Sci. 69, 79–96. doi:10.4141/cjss89-008.

Middleton, N., Sternberg, T., 2013. Climate hazards in drylands: A review. Earth-Sci. Rev. 126, 48–57. doi:10.1016/j.earscirev.2013.07.008.

Nickling, W.G., 1988. The initiation of particle movement by wind. Sedimentology 35, 499–511. doi:10.1111/j.1365-3091.1988.tb01000.x.

Nickling, W.G., Neuman, C.M., 1997. Wind tunnel evaluation of a wedge-shaped aeolian sediment trap. Geomorphology 18, 333. doi:10.1016/S0169-555X(96)00040-2.

Pye, K., Tsoar, H., 2009. Aeolian Sand and Sand Dunes. Springer. doi:10.1007/978-3-540-85910-9.

Raffaele, L., Bruno, L., Pellerey, F., Preziosi, L., 2016. Windblown sand saltation: A statistical approach to fluid threshold shear velocity. Aeolian Research 23, 79–91. doi:10.1016/j.aeolia.2016.10.002.

Redding, J.H., Lord, J.A., 1981. Designing for the effects of windblown sand along the new Jessah-Riyadh-Dammam expressway, in: Symposium on Geotechnical Problems in Saudi Arabia, pp. 363–395.

Repetto, M., Solari, G., 2004. Directional wind-induced fatigue of slender vertical structures. Journal of Structural Engineering 130, 1032–1040. doi:10.1061/~ASCE!0733-9445~2004!130:7~1032!

Riksen, M.J., Goossens, D., Huiskes, H., Krol, J., Slim, P., 2016. Constructing notches in foredunes: Effect on sediment dynamics in the dune hinterland. Geomorphology 15, 340–352. doi:10.1016/j.geomorph.2015.10.021.

Rizvi, A., 1989. Planning responses to aeolian hazards in arid regions. Journal of King Saud University, Architecture & Planning 1, 59–74.

Shao, Y., 2008. Physics and Modelling of Wind Erosion. Springer. doi:10.1007/978-1-4020-8895-7.

Shao, Y., Lu, H., 2000. A simple expression for wind erosion threshold friction velocity. J. Geophys. Res. 105, 22437–43. doi:10.1029/2000JD900304.

Sherman, D.J., Bailiang, L., Ellis, J.T., Farrell, E.J., Maia, L., Granja, H., 2013. Recalibrating aeolian sand transport models. Earth Surf. Process. Landforms 38, 169–178. doi:10.1002/esp.3310.

Sherman, D.J., Li, B., 2012. Predicting aeolian sand transport rates: A reevaluation of models. Aeolian Research 3, 371–378. doi:10.1016/j.aeolia.2011.06.002.

Stipho, A.S., 1992. Aeolian sand hazards and engineering design for desert regions. Quarterly Journal of Engineering Geology 25, 83–92. doi:10.1144/GSL.QJEG.1992.025.02.02.

Takle, E., Brown, J., 1978. Note on the use of weibull statistics to characterize wind-speed data. J. Appl. Meteorol. 17, 556–559. doi:10.1175/1520-0450(1978)017<0556:NOTUOW>2.0.CO;2.

Udo, K., 2009. New method for estimation of aeolian sand transport rate using ceramic sand flux sensor (ud-101). Sensors 9, 9058–9072. doi:10.3390/s91109058.

del Valle, H., Rostagno, C., Coronato, F., Bouza, P., Blanco, P., 2008. Sand dune activity in north-eastern Patagonia. Journal of Arid Environments 72, 411–422. doi:10.1016/j.jaridenv.2007.07.011.

Wang, X.M., Zhang, C.X., Hasi, E., Dong, Z.B., 2010. Has the Three Norths Forest Shelterbelt Program solved the desertification and dust storm problems in arid and semiarid China? Journal of Arid Environments 74, 13–22. doi:10.1016/j.jaridenv.2009.08.001.

Weaver, C.M., Wiggs, G.F.S., 2011. Field measurements of mean and turbulent airflow over a barchan sand dune. Geomorphology 128, 32–41. doi:10.1016/j.geomorph.2010.12.020.

Yang, X., Forman, S., Hu, F., Zhang, D., Liu, Z., Li, H., 2016. Initial insights into the age and origin of the Kubuqi sand sea of northern China. Geomorphology 259, 30–39. doi:10.1016/j.geomorph.2016.02.004.

Yang, Y., Qu, Z., Shi, P., Liu, L., Zhang, G., Tang, Y., Hu, X., Lv, Y., Xiong, Y., Wang, J., Shen, L., Lv, L., Sun, S., 2014. Wind regime and sand transport in the corridor between the Badain Jaran and Tengger deserts, central Alxa Plateau, China. Aeolian Research 12, 143–156. doi:10.1016/j.aeolia.2013.12.006.

Zakeri, J.A., 2012. Investigation on railway track maintenance in sandy-dry areas. Structure and Infrastructure Engineering: Maintenance, Management, Life-Cycle Design and Performance 8, 135–140. doi:10.1080/15732470903384921.

Zhang, C., Zou, X., Cheng, H., Yang, S., Pan, X., Liu, Y., Dong, G., 2007. Engineering measures to control windblown sand in shiquanhe town, tibet. J. Wind Eng. Ind. Aerod. 95, 53–70. doi:10.1016/j.jweia.2006.05.006.

Zhang, K.c., Qu, J.j., Liao, K.t., Niu, Q.h., Han, Q.j., 2010. Damage by wind-blown sand and its control along Qinghai-Tibet Railway in China. Aeolian Research 1, 143–146. doi:10.1016/j.aeolia.2009.10.001.

Zio, E., Pedroni, N., 2013. Literature review of methods for representing uncertainty. Foundation for an Industrial Safety Culture.